IEEE Photonics Journal
An IEEE Photonics Society Publication

Open Access

Design of Fabrication-Tolerant and Compact Waveguide Superconducting Single-Photon Detector Based on TM_0 Mode Absorption

Volume 13, Number 3, June 2021

Yang Li
Lue Tao
Yingxuan Zhao
Haiyang Huang
Xiaojuan She
Han Liao
Junbo Zhu
Zijian Zhu
Rui Huang
Xiang Liu
Fuwan Gan

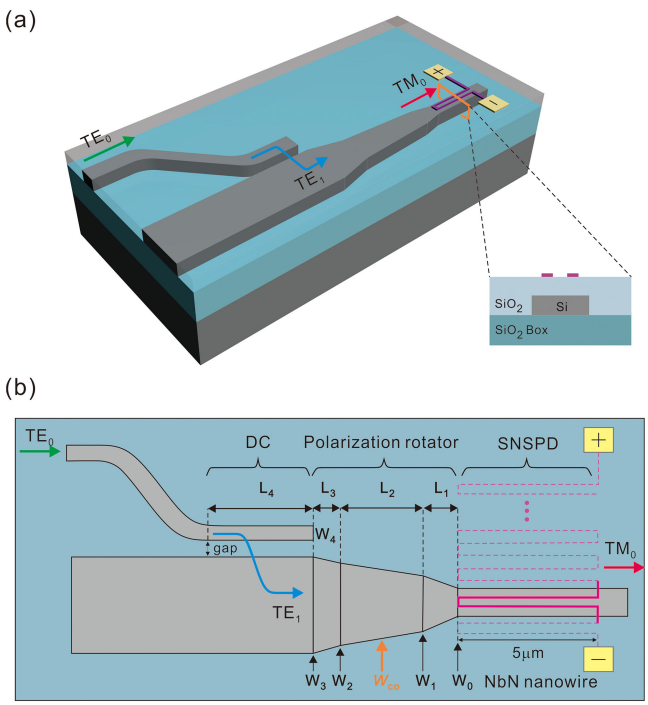

DOI: 10.1109/JPHOT.2021.3086868

Design of Fabrication-Tolerant and Compact Waveguide Superconducting Single-Photon Detector Based on TM_0 Mode Absorption

Yang Li,[1,2] **Lue Tao**,[1,2] **Yingxuan Zhao**,[1] **Haiyang Huang**,[1] **Xiaojuan She**,[1,2] **Han Liao**,[1,2] **Junbo Zhu**,[1,2] **Zijian Zhu**,[1,2] **Rui Huang**,[1,2] **Xiang Liu**,[1,2] **and Fuwan Gan**[2,3]

[1]State Key Laboratory of Functional Materials for Informatics, Shanghai Institute of Microsystem and Information Technology, Chinese Academy of Sciences, Shanghai 200050, China
[2]University of Chinese Academy of Sciences, Beijing 100049, China
[3]School of Future Technology, University of Chinese Academy of Sciences, Beijing 100049, China

DOI:10.1109/JPHOT.2021.3086868

Manuscript received April 19, 2021; revised May 30, 2021; accepted June 2, 2021. Date of publication June 7, 2021; date of current version June 22, 2021. This work was supported in part by the National Key Research and Development Program of China under Grant 2017YFA0206403, in part by the National Natural Science Foundation of China under Grant 61475180, in part by the Science and Technology Commission of Shanghai Municipality under Grant 16ZR1442600, in part by the Shanghai Municipal Science and Technology Major Project under Grant 2017SHZDZX03, in part by the Shanghai Sailing Program under Grant 18YF1428100, and in part by the Strategic Priority Research Program of Chinese Academy of Sciences under Grant XDB24020400. Corresponding author: Fuwan Gan (e-mail: fuwan@mail.sim.ac.cn).

Abstract: A TM_0 mode coupled travelling wave SNSPD based on SOI platform is designed. The light propagating in this device can achieve high-efficiency mode conversion from TE_0 mode to TM_0 mode and then absorbed by NbN nanowires on top of the waveguide. Thanks to the TM_0 mode coupled detection, the length of NbN nanowire that is needed to achieve a close-to-unity photon absorption is cut down to an extremely short level of $\sim$5 μm. Meanwhile, this TM_0 mode coupled travelling wave SNSPD is very robust against fabrication errors compared with TE_0 coupled SNSPD.

Index Terms: Travelling wave SNSPD, integrated quantum nanophotonic circuits, silicon-photonics, polarization rotator.

1. Introduction

Single photon detectors (SPDs) with high detection efficiency play a key role in modern quantum information [1] and measurement-based quantum applications such as quantum computation [2], [3], quantum key distribution [4], quantum simulating [5], loophole-free Bell experiments [6], [7] that utilize photons as quantum bits. Scalability is one of another most sought-after feature in monolithic integrated quantum nanophotonic circuits especially in the popular SOI platform. In the telecommunication wavelength regime around 1550 nm, avalanche photodiodes (APDs) such as InGaAs near-infrared photon detectors are predominantly. However, such detectors are plagued by

high dark count rates and low detection efficiency. What's more, these detectors are stand-alone which means they cannot be packaged to a scalable size.

In recent years, superconducting nanowire single-photon detector (SNSPD) has emerged and grown as a promising alternative photon detector, which exhibits high detecting efficiency, ultra-low noise, high counting rates and low timing jitter [8], [9]. SNSPDs usually utilize NbN (or NbTiN) as superconducting material, which operates at cryogenic environment below its critical temperature T_c. At this temperature, NbN nanowires are under superconductive state which means electrons flow under the nanowires without resistance. When photons are absorbed by NbN nanowires, hot-spot creation happens and locally destroys the superconductive state with a resistance area [10]. Current flow through this area will then registered electronically as pulses and thus provides a clear signature of photon detection events. However, traditional SNSPDs absorb photons coupled from normal incidence fibers which the detection efficiency is limited by the thickness of the thin NbN film (usually a few nanometers). Cavities [11], [12] or reflect mirrors [13], [14] can be used to enhance the absorption but they concomitantly reduces the optical bandwidth. Besides, the way of normal incidence still hinder these detectors from integrating to a nanophotonic circuit. In contrast, the waveguide travelling wave SNSPD [15]–[17] is a better choice because the superconducting NbN nanowires atop the waveguide can absorb the guided optical modes through evanescent wave coupling. In this way, the SNSPDs can achieve close-to-unity photon absorption on-chip as long as the NbN nanowire is long enough. Photon-number-resolving detectors (PNRDs) [18], spectrometers [19], and two photon interference (TPI) measurement [20] can also be realized in this travelling wave SNSPD scenario.

Unfortunately, most of the travelling wave SNSPDs need several tens of micrometer long of NbN nanowires to achieve close-to-unity absorption when dealing with the (quasi-) transverse electric (TE) modes. This will make the fabrication more difficult. Meanwhile, almost all of those SNSPDs deposit thin NbN film directly on the upper surface of core waveguide. It's efficient for light absorption but strict to the NbN nanowire etching process because once the etchant damages the core, the light inside the waveguide would be scattered at the rough upper surface.

Here, we propose a novel TM_0 mode coupled travelling wave SNSPD based on SOI platform with the NbN meander nanowires deposited on the surface of SiO_2 cladding. The SiO_2 cladding can protect the core waveguide from impact of the etchant and the quality of thin NbN film deposited on its surface will not be affected because of the advanced chemical mechanical polishing (CMP) technic. Moreover, for the sake of TM_0 mode coupled photon absorption, the length of NbN nanowire is reduced to an extremely short level ($\sim$5 μm) and the SNSPD is very robust against fabrication errors.

2. Design

The waveguide travelling wave SNSPD based on SOI platform has a single NbN nanowire, which is patterned into a meander shape. The cross section of the SNSPD is schematically shown in the inset of Fig. 1(a). The buried oxide layer is 2 μm thick and the core Si waveguide has a cross-section dimension of 500 nm $\times$ 220 nm. The NbN nanowires atop the SiO_2 cladding are 7 nm thick and 100 nm wide and are placed symmetrically above the Si core. NbN ($n = 5.23–5.82i$) [21] has a large imaginary part of refractive index so that a film of a few nanometer thick is enough to absorb the evanescent optical field. The real part of refractive index of NbN is also large, but due to the large area mismatch between the NbN nanowire and the core Si waveguide, the real part of the mode effective index of bare and NbN-covered waveguides are almost identical ($TE_0 < 0.2\%$, $TM_0 < 0.46\%$, obtained from Lumerical MODE solution). Therefore, the optical modes travel in the Si waveguide will experience a smooth transition between the two regions.

There are also two parameters that affect the NbN nanowire absorption: the spacing between the nanowires and the thickness of SiO_2 cladding. Considering the absorptance A in the NbN

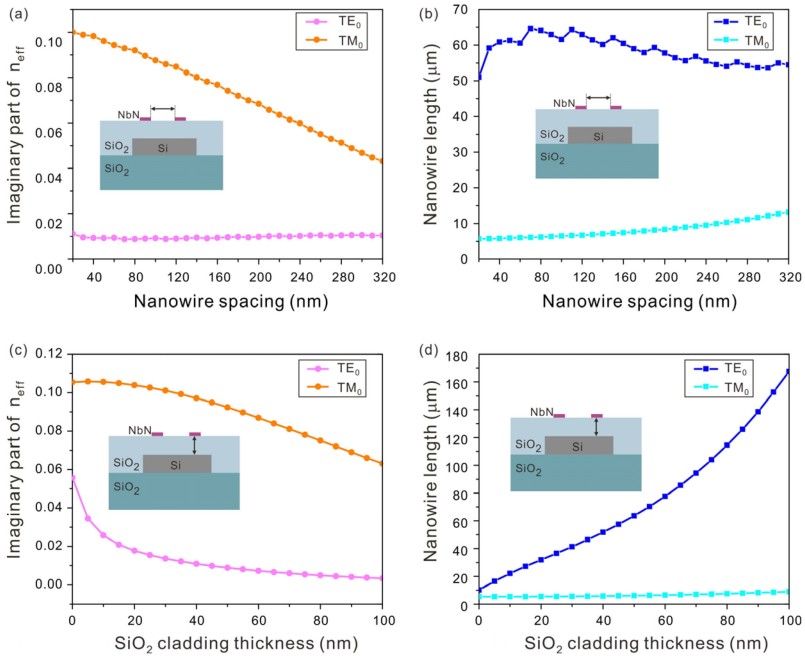

Fig. 1. The calculated imaginary part of TE_0 and TM_0 mode effective index and the nanowire length needed to achieve 99% light absorption when: (a)-(b) NbN nanowire spacing increases and (c)-(d) SiO_2 cladding thickness increases.

nanowires [22]:

$$\alpha = 2 \times \mathrm{Im}\left(\frac{2\pi}{\lambda} \times n_{eff}\right) \tag{1}$$

$$A = 1 - e^{-\alpha L} \tag{2}$$

Where α is an absorption coefficient, λ is the wavelength (1550 nm) of the guided light, n_{eff} is the mode effective index, L is the length of a single nanowire. First, the imaginary part of TE_0 and TM_0 mode effective index are plotted in Fig. 1(a) while the thickness of the SiO_2 cladding is 50 nm. Although the imaginary part of TM_0 mode effective index is decreased from 0.1 to 0.04 while the NbN nanowire spacing is increased from 20 nm to 320 nm, it is still several times bigger than that of TE_0 (< 0.011). Correspondingly, the nanowire length L calculated by equation (2) while A is set as 99% are plotted in Fig. 1(b), the TM_0 mode only needs $\sim$10 μm long nanowire to absorb 99% of the light while the TE_0 mode needs nearly 5 times longer. Furthermore, the TM_0 mode is more insensitive to the nanowire spacing variation than TE_0 mode. Since the width of core Si is only 500 nm, we set the nanowire spacing as 80 nm for easy fabrication. Second, we keep the nanowire spacing fixed at 80 nm and then calculate the imaginary part of mode effective index and nanowire length L for 99% absorptance by sweeping the cladding thickness from 0 nm to 100 nm. The results are shown in Fig. 1(c) and Fig. 1(d), respectively. Obviously, the TE_0 mode is very sensitive to cladding thickness while the TM_0 mode only needs < 10 μm to absorb 99% of the light even when the cladding thickness is 100 nm. Considering the difficulty of CMP process, we choose the cladding thickness as 50 nm.

Finally we set the spacing of the NbN nanowires 80 nm and the thickness of the SiO_2 cladding 50 nm, as shown in the inset of Fig. 2. The propagation of TE_0 mode and TM_0 mode in a 50 μm long waveguide covered with NbN nanowires are simulated by 3D FDTD method. The results are shown in Fig. 2. As we expected, TM_0 mode attenuates faster than TE_0 mode. More specifically, TM_0 mode only needs $\sim$5 μm to attenuate from 100% to less than 1% while TE_0 mode needs more

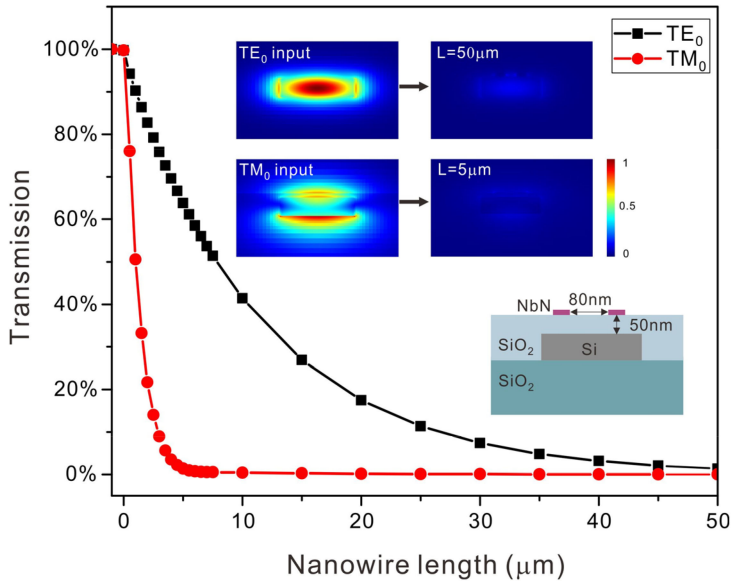

Fig. 2. The transmission of TE_0 and TM_0 mode lunched into a 50 μm long travelling wave SNSPD. Inset: upper: normalized electric field distribution of TE_0 and TM_0 input and when L = 50 μm and 5 μm, respectively; lower: the cross section of the travelling wave SNSPD.

than 50 μm to complete the same absorption. This is mainly affected by the different distributions of electric field. The electric field of TM_0 mode is polarized perpendicular to the upper surface of core waveguide which is more easily absorbed by NbN nanowires. The normalized electric field distribution of the input TE_0 mode and TM_0 mode and the electric field distribution after 99% absorption are shown in the inset of Fig. 2.

In photonic design, most of the nanophotonic circuits are based on (quasi-) TE modes for TM modes are lossy. Therefore, at the end of a chip, we designed a polarization rotator to convert TE_0 mode to TM_0 mode for detection. The TM_0 mode coupled travelling wave SNSPD is schematically shown in Fig. 3. The device is consist of three parts: (1) a directional coupler (DC), which can covert the TE_0 mode to TE_1 mode; (2) polarization rotator, which can convert the TE_1 mode to TM_0 mode; (3) SNSPD, which can absorb the TM_0 mode by evanescent wave coupling.

It's worth noting that for a short NbN nanowire, the count rate can be high, but very short nanowire will preclude operation of SNSPD resulting from a state called latching [23]. In real fabrication process, the latching can be avoid by increasing the kinetic inductance of NbN nanowire. According to the equation of kinetic inductance of SNSPD [24]:

$$L_k = \frac{\hbar R_n}{1.76\pi k T_c} \tag{3}$$

Where $R_n = \frac{l}{\sigma_n wd}$, σ_n is the conductivity in the normal state, l, w and d are the length, wire width and thickness of SNSPD respectively, k is the Boltzmann constant. The length of NbN nanowire can be adjusted by increasing the number of meander while keeping the effective length 5 μm on top of the Si waveguide, as shown in Fig. 3(b). We adjust the kinetic inductance of the SNSPD to make sure the thermal relaxation of the hotspot prior to the bias current I_b recovery and the latching can be avoid.

Polarization rotator is the core part of the device. Waveguide-type polarization rotators are difficult to realize because it is not easy to rotate the optical axis of a planar waveguide. In order to realize polarization rotation, we have to break the symmetry of vertical refractive index with structures like bi-level tapers [25], [26], horizontal slot waveguides [27], stacked waveguides [28], and core waveguide with a cut corner [29], [30] etc. These structures usually unavoidably increase

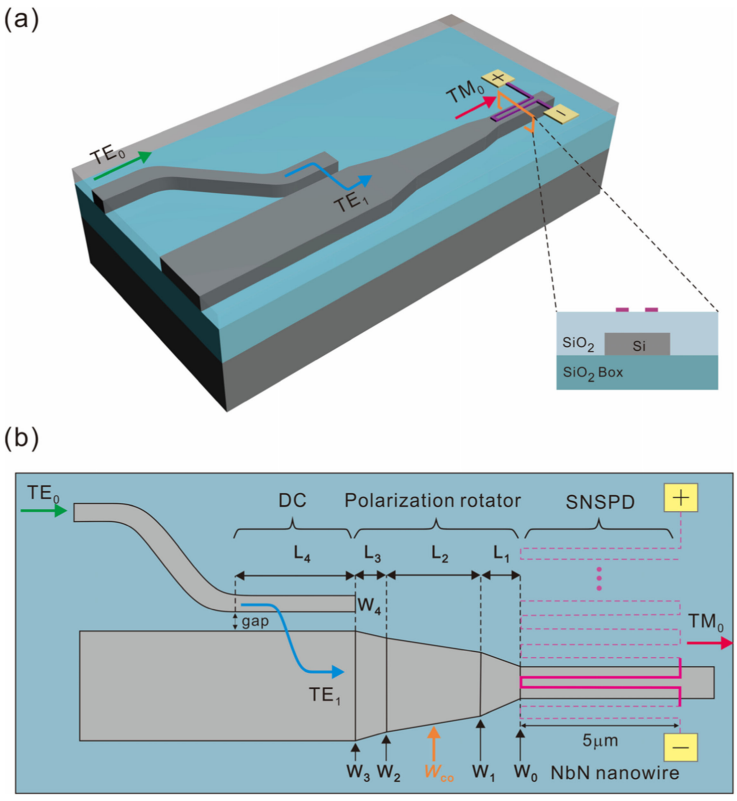

Fig. 3. Schematic configuration of the TM_0 mode coupled travelling wave SNSPD. (a) 3D view; (b) top view.

the fabrication complexity, e.g., double etching process, multi materials deposition and precise aligning requirement. In this paper, we achieve the polarization rotation by using three cascaded tapers in a SOI chip, where the vertical refractive index symmetry is broken by reducing the SiO_2 cladding thickness to 50 nm. Furthermore, only one-step etching is needed, which is compatible with standard nanophotonic circuits fabrication process.

We simulated 220 nm thick core Si with different cladding materials and thickness. The refractive index of Si, SiO_2 and Si_3N_4 are 3.476, 1.444 and 1.979, respectively. Fig. 4 shows the effective mode index evolution of TE_0, TM_0 and TE_1 mode as the core waveguide width W_{co} increases from 0.3 μm to 1.5 μm. When the SiO_2 cladding is 3 μm thick (shown in Fig. 4(a)), the refractive index in vertical is symmetrical and therefore the eigenmodes of TE_0, TM_0 and TE_1 are purely polarized. However, when the cladding material is air ($n = 1$) or 3 μm thick Si_3N_4, the modes are hybrid, as labeled with dashed circle in Fig. 4(b)-(c), and one cannot distinguish them at some special W_{co}. For the travelling wave SNSPD structure, the SiO_2 cladding thickness is reduced to 50 nm and the mode hybridization between TE_1 and TM_0 still exists, as shown in Fig. 4(d). This phenomenon demonstrates that cladding thickness is another factor to influence the mode hybridization besides material. The mode hybridization in these structures can be used as a polarization rotator, when light propagates along an adiabatic taper, the mode conversion between TE_1 mode and TM_0 mode happens [26].

It's feasible combining the waveguide type polarization rotator with the travelling wave SNSPD to accomplish a TM_0 mode coupled SNSPD. The polarization rotator shown in Fig. 3(b) is consist of three cascaded tapers. The length L_2 should be long enough to keep the mode conversion adiabatically, meanwhile the width of the two ends (w_1, w_2) must cover the mode transition point ($W_{co} = 0.63$ μm) which we choose from Fig. 3(d). Therefore we choose $w_1 = 0.56$ μm and $w_2 =$

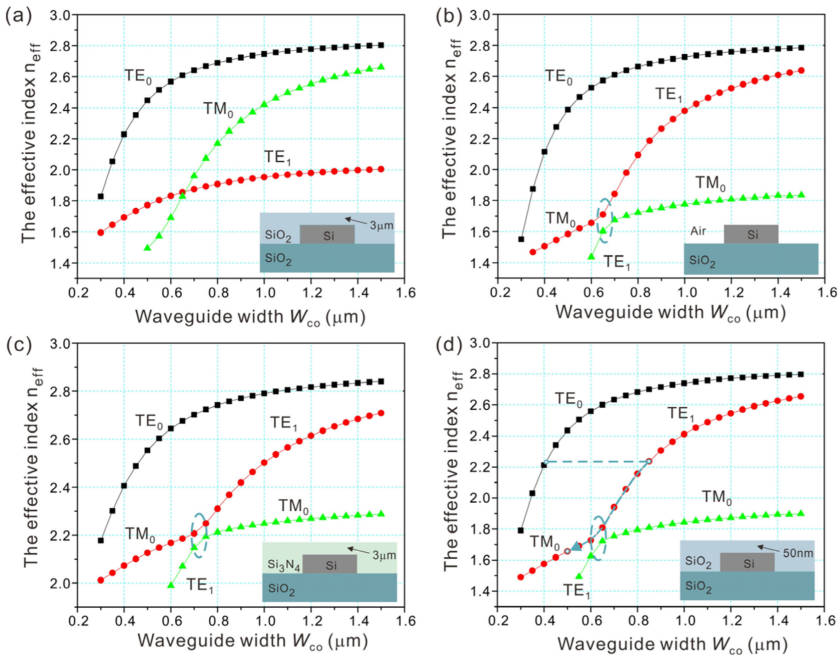

Fig. 4. The calculated mode effective indices of eigenmodes TE_0, TM_0, TE_1 with (a) 3 μm thick SiO_2; (b) air; (c) 3 μm thick Si_3N_4; (d) 50 nm thick SiO_2 upper claddings.

0.7 μm to satisfy $w_1 < w_{co} < w_2$, $w_0 = 0.5$ μm to match the travelling wave SNSPD structure and $w_3 = 0.85$ μm to avoid the mode hybridization. In order to obtain high mode conversion efficiency and keep the device compact, the L_1, L_2, L_3 should be carefully optimized. In this paper, we set $L_1 = 1$ μm, 2 μm, 3 μm, 4 μm, 5 μm, 10 μm and corresponding $L_3 = 2.5$ μm, 5 μm, 7.5 μm, 10 μm, 12.5 μm, 25 μm ($L_3 = L_1$ (w_3-w_2)/ (w_1-w_0)) because the first and third taper are used to bridge the adjacent segments which won't influence the conversion efficiency greatly. For different combinations of length L_1 and L_3, the length L_2 is optimized for maximum mode conversion efficiency as shown in Fig. 5. There are some ripples in these curves and even obvious as the L_1 length decreases. This is caused by the uncomplete mode conversion in the first and third taper because they are too short. Fortunately, we can always get high polarization conversion efficiency (~100%) from TE_1 mode to TM_0 mode as long as we choose the L_2 length properly. In our design, we choose $L_2 = 46$ μm, $L_1 = 4$ μm and corresponding $L_3 = 10$ μm for high mode conversion efficiency while the device is still compact. The inset of Fig. 5 shows the filed intensity distribution when TE_1 mode is lunched as input and propagates in this polarization rotator. From the electric field distribution evolution, we can clearly see that the TE_1 mode convert to TM_0 mode with conversion efficiency of ~98%.

The DC part of this device is to convert TE_0 mode to TE_1 mode. A directional coupler is designed so that the TE_0 mode in the upper narrow waveguide could be coupled to TE_1 mode in the lower wide waveguide based on the mode coupling theory. The width w_3 is fixed as 0.85 μm, and we choose $w_4 = 0.41$ μm to satisfy the phase matching condition, i.e., n_{eff}_TE_0 (w_4) = n_{eff}_TE_1 (w_3), which is marked by the dotted line in Fig. 4(d). We calculated the coupling efficiency as the coupling length L_4 increases from 0 μm to 30 μm while the gap is set as 0.1 μm, 0.15 μm, 0.2 μm and 0.25 μm. The results are shown in Fig. 6. For any gap width, there are optimal coupling lengths for maximal coupling efficiency and the optimal coupling length decreases as the gap decreases. Here we choose the coupling gap as 0.15 μm and corresponding L_4 length of 13 μm for a good tradeoff between a compact size and a UV lithography compatible patterning linewidth.

Fig. 7 shows the intensity of light propagating along the whole device when TE_0 mode is lunched as input mode. We mesh the NbN thin film with a 1 nm grid for it's only 7 nm thick. The normalized

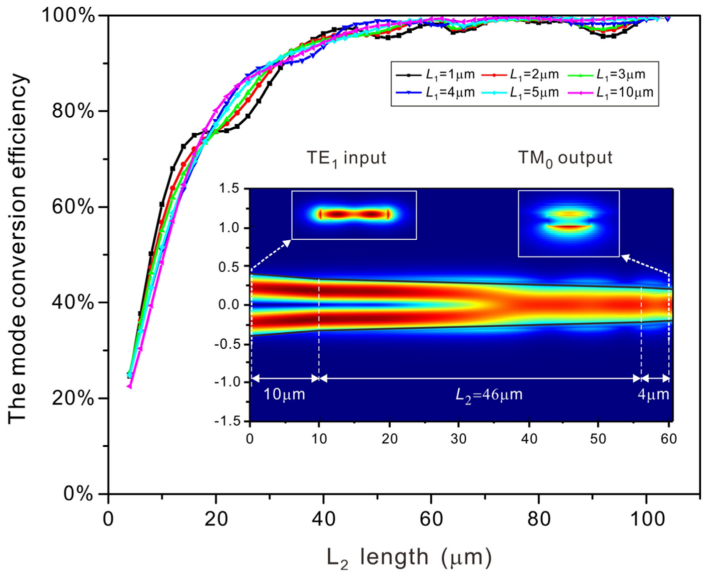

Fig. 5. The mode conversion efficiency from TE_1 to TM_0 as L_2 length increases with different L_1, L_3 combinations. Inset: the intensity of light propagating through the polarization rotator and the electric field distribution at the input and output port.

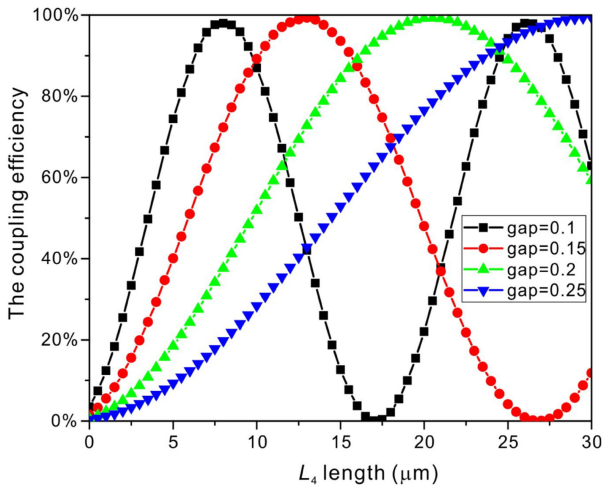

Fig. 6. The coupling efficiency as L_4 length increases with different gaps.

electric field distribution at some important nodes are also shown, from where we can clearly see the mode is converted from TE_0 to TM_0 and finally absorbed by 5 μm long NbN nanowire (labeled by purple line). The transition at these nodes are shown at the bottom of the electric field distributions, which is in good agreement with our expectation.

SNSPD is a wide range detector spanning UV to mid-IR wavelength [31] and the imaginary part index of NbN is large enough around 1550 nm [32], so we calculated the wavelength dependence of the TM_0 mode coupled travelling wave SNSPD. Fig. 8 shows the wavelength dependence of the directional coupler, polarization rotator and the whole device (including NbN nanowire) when TE_0 mode lunched as input, respectively. We can see that the bandwidth of the device is mainly limited by the directional coupler. But it still shows a 0.5dB loss in the bandwidth of $\sim$70 nm and 1dB loss in the bandwidth of $\sim$100 nm around 1550 nm.

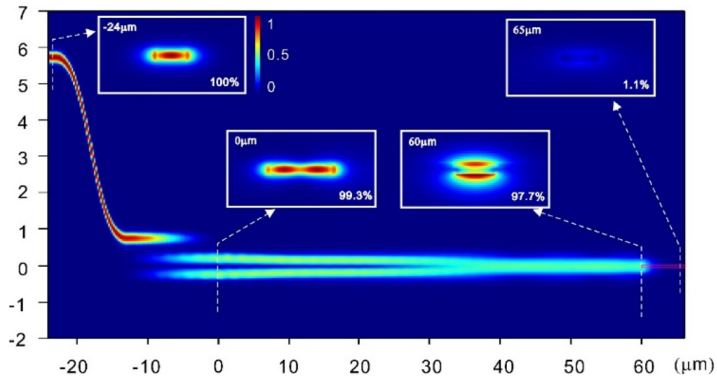

Fig. 7. The intensity of light propagating along the device when TE_0 mode lunched as input. Inset: normalized electric field distribution and transition at some important nodes.

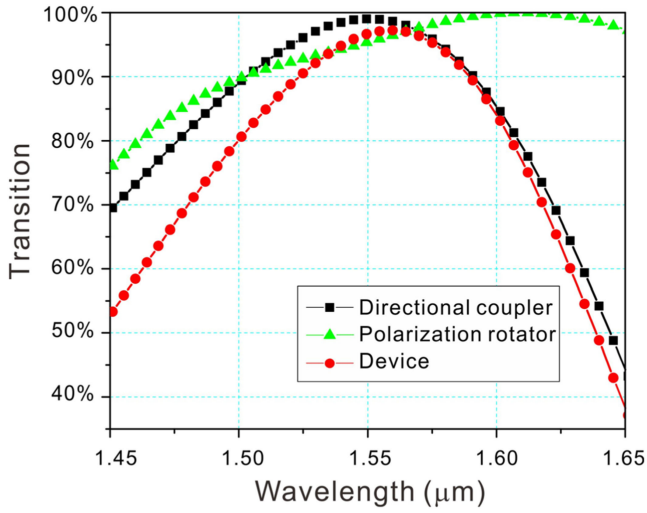

Fig. 8. The wavelength dependence of the TM_0 mode coupled travelling wave SNSPD.

3. Conclusion

In this paper, we designed a TM_0 mode coupled travelling wave SNSPD based on SOI platform simulated by commercial software Lumerical (Lumerical Solutions, Inc., London, U.K.). When TE_0 mode lunched into the device, it will coupled to TE_1 mode in the adjacent waveguide through a 13 μm long directional coupler with a 150 nm gap. Then three cascaded tapers adiabatically covert the TE_1 mode into TM_0 mode with high conversion efficiency close to 100%. Finally, a $\sim$5 μm NbN nanowire atop the waveguide absorb the TM_0 mode through waveguide evanescent wave coupling with an absorptance close-to-unity. Thanks to the novel way of TM_0 mode coupled absorption, the SNSPD is short enough and is very robust against fabrication errors compared with TE_0 mode coupled SNSPD. Moreover, we innovatively deposit the NbN thin film on the surface of SiO_2 cladding, which can protect the core waveguide from damage during the NbN etching process. Compared with traditional waveguide fabrication process, only one extra fabrication step (CMP) is added and it's easy to do. More importantly, our design simplify the NbN nanowire fabrication process greatly, which we think it's a good tradeoff between nanowire fabrication and waveguide fabrication. The TM_0 mode coupled travelling wave SNSPD we proposed could be helpful in the future monolithic integrated photonic quantum circuits to simplify the NbN nanowire fabrication process.

References

[1] N. Gisin *et al.*, "Quantum cryptography," *Rev. Modern Phys.*, vol. 74, no. 1, pp. 145–195, 2002.
[2] H. J. Briegel *et al.*, "Measurement-based quantum computation," *Nature Phys.*, vol. 5, no. 1, pp. 19–26, 2009.
[3] E. Knill, R. Laflamme, and G. J. Milburn, "A scheme for efficient quantum computation with linear optics," *Nature*, vol. 409, no. 6816, pp. 46–52, 2001.
[4] H. L. Yin *et al.*, "Measurement-device-independent quantum key distribution over a 404 km optical fiber," *Phys. Rev. Lett.*, vol. 117, no. 19, 2016, Art. no. 190501.
[5] H. Wang *et al.*, "Toward scalable boson sampling with photon loss," *Phys. Rev. Lett.*, vol. 120, no. 23, 2018, Art. no. 230502.
[6] L. K. Shalm *et al.*, "Strong loophole-free test of local realism," *Phys. Rev. Lett.*, vol. 115, no. 25, 2015, Art. no. 250402.
[7] B. G. Christensen *et al.*, "Detection-loophole-free test of quantum nonlocality, and applications," *Phys. Rev. Lett.*, vol. 111, no. 13, 2013, Art. no. 130406.
[8] G. N. Gol'tsman *et al.*, "Picosecond superconducting single-photon optical detector," *Appl. Phys. Lett.*, vol. 79, no. 6, pp. 705–707, 2001.
[9] L. You, "Superconducting nanowire single-photon detectors for quantum information," *Nanophotonics*, vol. 9, no. 9, pp. 2673–2692, 2020.
[10] C. M. Natarajan, M. G. Tanner, and R. H. Hadfield, "Superconducting nanowire single-photon detectors: Physics and applications," *Superconductor Sci. Technol.*, vol. 25, no. 6, 2012, Art. no. 063001.
[11] K. M. Rosfjord *et al.*, "Nanowire single-photon detector with an integrated optical cavity and anti-reflection coating," *Opt Exp.*, vol. 14, no. 2, pp. 527–534, 2006.
[12] I. Milostnaya *et al.*, "Superconducting single-photon detectors designed for operation at 1.55-μm telecommunication wavelength," *J. Phys.: Conf. Ser.*, vol. 43, pp. 1334–1337, 2006.
[13] P. Hu *et al.*, "Detecting single infrared photons toward optimal system detection efficiency," *Opt Exp.*, vol. 28, no. 24, pp. 36884–36891, 2020.
[14] W. Zhang *et al.*, "NbN superconducting nanowire single photon detector with efficiency over 90% at 1550 nm wavelength operational at compact cryocooler temperature," *Sci. China Phys. Mech. Astron.*, vol. 60, no. 12, 2017, Art. no. 120314.
[15] J. P. Sprengers *et al.*, "Waveguide superconducting single-photon detectors for integrated quantum photonic circuits," *Appl. Phys. Lett.*, vol. 99, no. 18, 2011, Art. no. 181110.
[16] W. H. Pernice *et al.*, "High-speed and high-efficiency travelling wave single-photon detectors embedded in nanophotonic circuits," *Nature Commun.*, vol. 3, 2012, Art. no. 1325.
[17] O. Kahl *et al.*, "Waveguide integrated superconducting single-photon detectors with high internal quantum efficiency at telecom wavelengths," *Sci. Rep.*, vol. 5, 2015, Art. no. 10941.
[18] D. Sahin *et al.*, "Waveguide photon-number-resolving detectors for quantum photonic integrated circuits," *Appl. Phys. Lett.*, vol. 103, no. 11, 2013, Art. no. 111116.
[19] O. Kahl *et al.*, "Spectrally multiplexed single-photon detection with hybrid superconducting nanophotonic circuits," *Optica*, vol. 4, no. 5, 2017, Art. no. 557.
[20] C. Schuck *et al.*, "Quantum interference in heterogeneous superconducting-photonic circuits on a silicon chip," *Nature Commun.*, vol. 7, 2016, Art. no. 10352.
[21] V. Anant *et al.*, "Optical properties of superconducting nanowire single-photon detectors," *Opt Exp.*, vol. 16, no. 14, pp. 10750–10761, 2008.
[22] L. You *et al.*, "Microfiber-coupled superconducting nanowire single-photon detector for near-infrared wavelengths," *Opt Exp.*, vol. 25, no. 25, pp. 31221–31229, 2017.
[23] A. J. Annunziata *et al.*, "Reset dynamics and latching in niobium superconducting nanowire single-photon detectors," *J. Appl. Phys.*, vol. 108, no. 8, 2010, Art. no. 084507.
[24] L. You, X. Shen, and X. Yang, "Single photon response of superconducting nanowire single photon detector," *Chin. Sci. Bull.*, vol. 55, no. 4/5, pp. 441–445, 2010.
[25] N. N. FENG *et al.*, "Low-loss compact-size slotted waveguide polarization rotator and transformer," *Opt. Lett.*, vol. 32, no. 15, pp. 2131–2133, 2007.
[26] D. Dai, Y. Tang, and E. Bowers J, "Mode conversion in tapered submicron silicon ridge optical waveguides," *Opt Exp.*, vol. 20, no. 12, pp. 13425–13439, 2012.
[27] H. Zhang *et al.*, "Efficient and broadband polarization rotator using horizontal slot waveguide for silicon photonics," *Appl. Phys. Lett.*, vol. 101, no. 2, 2012, Art. no. 021105.
[28] L. Chen, C. R. Doerr, and Y. K. Chen, "Compact polarization rotator on silicon for polarization-diversified circuits," *Opt. Lett.*, vol. 36, no. 4, pp. 469–471, 2011.
[29] Z. Wang and D. Dai, "Ultrasmall Si-nanowire-based polarization rotator," *J. Opt. Soc. Amer. B*, vol. 25, no. 5, 2008, Art. no. 747.
[30] M. Aamer *et al.*, "CMOS compatible silicon-on-insulator polarization rotator based on symmetry breaking of the waveguide cross section," *IEEE Photon. Technol. Lett.*, vol. 24, no. 22, pp. 2031–2034, Nov. 2012.
[31] R. Lusche *et al.*, "Effect of the wire width on the intrinsic detection efficiency of superconducting-nanowire single-photon detectors," *J. Appl. Phys.*, vol. 116, no. 4, 2014, Art. no. 043906.
[32] A. Banerjee *et al.*, "Optical properties of refractory metal based thin films," *Opt. Mater. Exp.*, vol. 8, no. 8, 2018, Art. no. 2072.